Simultaneous multi-lifetime multi-color STED imaging for colocalization analyses

Johanna Bückers, Dominik Wildanger, Giuseppe Vicidomini, Lars Kastrup, and Stefan W. Hell*

Department of NanoBiophotonics, Max Planck Institute for Biophysical Chemistry, Am Fassberg 11, 37077 Göttingen, Germany
**shell@gwdg.de*

Abstract: We describe a STED microscope optimized for colocalization experiments with up to three colors. Two fluorescence labels are separated by their fluorescence lifetime whereas a third channel is discriminated by the wavelength of fluorescence emission. Since it does not require a second STED beam, separating by lifetime is insensitive to drift and thus optimally suited for colocalization analyses. Furthermore, we propose a setup having a second STED beam for long duration multicolor recording.

OCIS codes: (180.2520) Fluorescence microscopy; (350.5730) Resolution.

References and links

1. T. Foerster, "Intermolecular energy migration and fluorescence," Ann. Phys. **2**, 55 (1948).
2. P. Wu, and L. Brand, "Resonance energy transfer: methods and applications," Anal. Biochem. **218**(1), 1–13 (1994).
3. C. D. Hu, Y. Chinenov, and T. K. Kerppola, "Visualization of interactions among bZIP and Rel family proteins in living cells using bimolecular fluorescence complementation," Mol. Cell **9**(4), 789–798 (2002).
4. T. K. Kerppola, "Design and implementation of bimolecular fluorescence complementation (BiFC) assays for the visualization of protein interactions in living cells," Nat. Protoc. **1**(3), 1278–1286 (2006).
5. K. Carlsson, and A. Liljeborg, "Confocal fluorescence microscopy using spectral and lifetime information to simultaneously record four fluorophores with high channel separation," J. Microsc. **185**(1), 37–46 (1997).
6. R. E. Thompson, D. R. Larson, and W. W. Webb, "Precise nanometer localization analysis for individual fluorescent probes," Biophys. J. **82**(5), 2775–2783 (2002).
7. K. I. Willig, S. O. Rizzoli, V. Westphal, R. Jahn, and S. W. Hell, "STED microscopy reveals that synaptotagmin remains clustered after synaptic vesicle exocytosis," Nature **440**(7086), 935–939 (2006).
8. V. Zinchuk, O. Zinchuk, and T. Okada, "Quantitative Colocalization Analysis of Multicolor Confocal Immunofluorescence Microscopy Images: Pushing Pixels to Explore Biological Phenomena," Acta Histochem. Cytochem. **40**(4), 101–111 (2007).
9. S. W. Hell, "Microscopy and its focal switch," Nat. Methods **6**(1), 24–32 (2009).
10. S. W. Hell, and J. Wichmann, "Breaking the diffraction resolution limit by stimulated emission: stimulated-emission-depletion fluorescence microscopy," Opt. Lett. **19**(11), 780–782 (1994).
11. J. Keller, A. Schönle, and S. W. Hell, "Efficient fluorescence inhibition patterns for RESOLFT microscopy," Opt. Express **15**(6), 3361–3371 (2007).
12. E. Betzig, G. H. Patterson, R. Sougrat, O. W. Lindwasser, S. Olenych, J. S. Bonifacino, M. W. Davidson, J. Lippincott-Schwartz, and H. F. Hess, "Imaging intracellular fluorescent proteins at nanometer resolution," Science **313**(5793), 1642–1645 (2006).
13. S. T. Hess, T. P. K. Girirajan, and M. D. Mason, "Ultra-High Resolution Imaging by Fluorescence Photoactivation Localization microscopy," Biophys. J. **91**(11), 4258–4272 (2006).
14. M. J. Rust, M. Bates, and X. W. Zhuang, "Sub-diffraction-limit imaging by stochastic optical reconstruction microscopy (STORM)," Nat. Methods **3**(10), 793–796 (2006).
15. A. Egner, C. Geisler, C. von Middendorff, H. Bock, D. Wenzel, R. Medda, M. Andresen, A. C. Stiel, S. Jakobs, C. Eggeling, A. Schönle, and S. W. Hell, "Fluorescence nanoscopy in whole cells by asynchronous localization of photoswitching emitters," Biophys. J. **93**(9), 3285–3290 (2007).
16. S. van de Linde, R. Kasper, M. Heilemann, and M. Sauer, "Photoswitching microscopy with standard fluorophores," Appl. Phys. B **93**(4), 725–731 (2008).
17. W. Heisenberg, *The Physical Principles of the Quantum Theory* (Chicago University Press, 1930).
18. M. Bates, B. Huang, G. T. Dempsey, and X. W. Zhuang, "Multicolor Super-Resolution Imaging with Photo-Switchable Fluorescent Probes," Science **317**(5845), 1749–1753 (2007).
19. G. Donnert, J. Keller, C. A. Wurm, S. O. Rizzoli, V. Westphal, A. Schönle, R. Jahn, S. Jakobs, C. Eggeling, and S. W. Hell, "Two-Color Far-Field Fluorescence Nanoscopy," Biophys. J. **92**(8), L67–L69 (2007).

#140586 - $15.00 USD Received 4 Jan 2011; accepted 18 Jan 2011; published 2 Feb 2011

20. H. Shroff, C. G. Galbraith, J. A. Galbraith, H. White, J. Gillette, S. Olenych, M. W. Davidson, and E. Betzig, "Dual-color superresolution imaging of genetically expressed probes within individual adhesion complexes," Proc. Natl. Acad. Sci. U.S.A. **104**(51), 20308–20313 (2007).
21. M. Bossi, J. Folling, V. N. Belov, V. P. Boyarskiy, R. Medda, A. Egner, C. Eggeling, A. Schonle, and S. W. Hell, "Multi-color far-field fluorescence nanoscopy through isolated detection of distinct molecular species," Nano Lett. **8**(8), 2463–2468 (2008).
22. V. Westphal, S. O. Rizzoli, M. A. Lauterbach, D. Kamin, R. Jahn, and S. W. Hell, "Video-Rate Far-Field Optical Nanoscopy Dissects Synaptic Vesicle Movement," Science **320**(5873), 246–249 (2008).
23. J. Engelhardt, J. Keller, P. Hoyer, M. Reuss, T. Staudt, and S. W. Hell, "Molecular Orientation Affects Localization Accuracy in Superresolution Far-Field Fluorescence Microscopy," Nano Lett. (2010).
24. D. Wildanger, E. Rittweger, L. Kastrup, and S. W. Hell, "STED microscopy with a supercontinuum laser source," Opt. Express **16**(13), 9614–9621 (2008).
25. D. Wildanger, R. Medda, L. Kastrup, and S. W. Hell, "A compact STED microscope providing 3D nanoscale resolution," J. Microsc. **236**(1), 35–43 (2009).
26. E. Auksorius, B. R. Boruah, C. Dunsby, P. M. P. Lanigan, G. Kennedy, M. A. A. Neil, and P. M. W. French, "Stimulated emission depletion microscopy with a supercontinuum source and fluorescence lifetime imaging," Opt. Lett. **33**(2), 113–115 (2008).
27. M. Maus, M. Cotlet, J. Hofkens, T. Gensch, F. C. De Schryver, J. Schaffer, and C. A. Seidel, "An experimental comparison of the maximum likelihood estimation and nonlinear least-squares fluorescence lifetime analysis of single molecules," Anal. Chem. **73**(9), 2078–2086 (2001).
28. K. Carlsson, N. Aslund, K. Mossberg, J. Philip, M. Maus, M. Cotlet, J. Hofkens, T. Gensch, F. C. De Schryver, J. Schaffer, and C. A. Seidel, "Simultaneous confocal recording of multiple fluorescent labels with improved channel separation," J. Microsc. **176**(Pt 3), 287–299 (1994).
29. R. Neher, and E. Neher, "Optimizing imaging parameters for the separation of multiple labels in a fluorescence image," J. Microsc. **213**(1), 46–62 (2004).
30. D. Neumann, J. Bückers, L. Kastrup, S. W. Hell, and S. Jakobs, "Two-color STED microscopy reveals different degrees of colocalization between hexokinase-I and the three human VDAC isoforms," PMC Biophys **3**(1), 1–4 (2010).

1. Introduction

A common problem studied with fluorescence microscopy is the interplay between two or more proteins in a cellular environment. Usually, one is interested in whether a certain cellular function is mediated by the binding of two or more proteins. Besides Förster resonance energy transfer (FRET) [1,2] and bimolecular fluorescence complementation (BiFC) [3,4] the colocalization of proteins is often investigated with two- (or multi-)color fluorescence imaging. In multicolor imaging the individual targets are tagged with fluorophores of different color and subsequently detected in separate color channels in order to analyze their spatial distribution. Such studies are usually performed with confocal microscopes [5] having a spatial resolution limited to ~250 nm by diffraction. While the position and thus the degree of co-localization of two disparate (e.g. differently labeled) point objects can be determined down to a few nanometers by centroid calculations [6], it is not straightforward to find out if the co-localization occurs between two extended, arbitrarily shaped objects or between multiple objects consisting of individual clusters as is often the case with proteins [7]. Another complication arising due to the limited spatial resolution is the overlap of fluorescence between separate color channels which is used to quantify the degree of protein colocalization [8]; two features may well overlap in the (confocal) images but may still be separated by 50–100 nm in space. Finally, in most applications it is important to find out where exactly the co-localizing proteins are located in the cell. Therefore, in most cases it is not sufficient to establish the degree of overlap between different color channels, but one requires high resolution as well. So, in order to obtain meaningful colocalization information, it is inevitable to image with subdiffraction resolution.

Having turned into nanoscopy, modern fluorescence microscopy has overcome the diffraction barrier and allows imaging at a spatial resolution down to 20 nm and beyond [9]. What distinguishes the novel concepts from traditional optical imaging is the exploitation of the photophysical properties of the fluorescent label into the image formation process [9]. In particular, all nanoscopy concepts in use today, in one way or the other make sure that not all emitters residing within the diffraction range are able to emit simultaneously [9]. To this end a molecular transition is employed ensuring that only a fraction of fluorophores (down to a single one) is able to respond with fluorescence when exposed to excitation light. The other

#140586 - $15.00 USD Received 4 Jan 2011; accepted 18 Jan 2011; published 2 Feb 2011

fluorophores residing within the diffraction range remain dark. Thus, features can be separated due to their time-sequential signaling.

Stimulated emission depletion (STED) microscopy [10] silences (switches off) fluorophores by means of a beam inducing stimulated emission from the excited state to the ground state. In a typical setup, the wavefront of this so-called STED beam is modified such that a doughnut-shaped focal spot of STED light is formed [11] and overlapped with a regularly focused excitation beam. In most of the area covered by the doughnut, the focal intensity of the STED beam is beyond the level at which the dye can spend significant time in the fluorescent state. Since they cannot reside in the fluorescent state, virtually all fluorophores are turned off except those in close proximity to the doughnut minimum (where the STED beam intensity is below the threshold). Scanning the beams across the sample sequentially turns off the signaling of adjacent fluorophores, thus allowing the separation of features at subdiffraction distances and, thus, the recording of a subdiffraction image.

In the second major group of high-resolution methods (PALM [12,13], STORM [14], GSDIM [15] and variants thereof [16]) all fluorophores are forced to reside in a non-emissive state and, at each instant, only a single molecule per diffraction range is enabled to emit by a photoinduced (PALM, STORM) or spontaneous transition (GSDIM) out of the non-fluorescent state. Because only a single molecule is fluorescent at any time within the diffraction range, their separation on a camera is not challenged by diffraction; moreover, each molecule can be assigned a precise position calculated from the centroid of its fluorescence signature [17,6]. The process is repeated for all – or at least for a representative number of molecules within a diffraction range in the sample until a high-resolution image emerges from the individual position measurements.

Both STED and PALM/STORM microscopes can be implemented as multicolor instruments [18–20]. Upgrading single-molecule switching microscopes to multicolor operation is particularly convenient because it requires just the addition of a beamsplitter in the detection path and, if applicable, an additional excitation laser. With two spectral detection windows more than just two colors can be discriminated because fluorescent dyes with different emission spectra give rise to dissimilar and unique brightness ratios in the two detection windows by which they can be classified [21]. Implementing a two-color STED microscope is slightly more complex due to the multiple wavelengths involved (for excitation, emission and for STED). It thus requires a more careful design of the beamsplitters and a more careful combination of dyes. In particular, care must be taken not to excite the longer-wavelength dye with the shorter-wavelength (high power) STED beam.

Generally, in order for colocalization analyses to be meaningful down to the nanometer scale, particular attention must be paid to the design of the microscope and of the experiment. To minimize the influence of thermal drift and mechanical creeping, image acquisition should be fast and the color channels should be recorded in parallel rather than sequentially. This ensures that closely spaced features are imaged within a short time interval. Fast and simultaneous imaging is of particular importance when living specimens are investigated; they inevitably introduce motion artifacts if the recording is not significantly faster than the specimen motion.

For all these reasons, STED microscopy has key advantages when it comes to colocalization applications. A strength of a coordinate-targeted nanoscopy modality such as STED is that it can operate at relatively high imaging speed [9,22].Moreover, as it has been detailed recently [23], the (co-)localization of individual fluorescent molecules in non-surface bound PALM, STORM, GSDIM and related concepts is severely compromised by the orientation of the emission dipole. While the localization error is small if the emission dipole can rotate freely, the apparent position of a fixed emitter can deviate up to ~125 nm from the real position in these single molecule based nanoscopy concepts [23]. Unless precise knowledge about the fluorophore mobility or orientation is available (which is rarely the case) the uncertainty due to orientational effects can degrade the images and compromise the colocalization analyses. In STED microscopy, the dipole orientation also affects the resolution because the interaction of the STED light with the fluorophore is subject to

#140586 - $15.00 USD Received 4 Jan 2011; accepted 18 Jan 2011; published 2 Feb 2011

photoselection. However, the mere decrease in resolution does not compromise the colocalization analysis because the position of the features in the images is not shifted; the position is predefined by the intensity minimum of the STED beam.

When using STED microscopy the accuracy of a colocalization analysis is only limited by the precision with which the STED foci can be superimposed. In fact, an optimal implementation would not require multiple STED beams but rely on a single one. Therefore, in order to achieve the highest colocalization accuracy possible, we decided to use two fluorescent dyes with nearly identical absorption and emission spectra but with different fluorescent lifetimes which allowed us to use common excitation and STED beams and to separate the channels by their fluorescence lifetimes. This design intrinsically provides high spatial resolution and, because the channels are recorded simultaneously, it is insensitive to artifacts induced by drift. We further extended the microscope to three-color imaging by combining the lifetime-based separation with a spectral separation, which still required the addition of a second pair of excitation and STED beams.

2. Materials and methods

2.1 Optical setup

The images were recorded with a custom-built STED microscope combining two pairs of excitation and STED laser beams, all stemming from a single supercontinuum laser source [24,25]. Whereas the excitation wavelengths (570±2 nm and 650±2 nm) were selected from the supercontinuum using an acousto-optical tunable filter (AOTF, AA Opto-Electronic, Orsay Cedex, France) the STED wavelengths (720±10 nm, 755±15 nm) were extracted using prism monochromators ensuring strict wavelength selections. After filtering the appropriate wavelength ranges, the four beams were coupled into separate polarization-maintaining single mode fibers. At the fiber outputs the beams were collimated and sent to the objective lens. The corresponding excitation and STED beams were combined using dichroic mirrors to give two pairs of beams with orthogonal polarization. The beam pairs were then combined with a polarizing beam splitter cube and coupled into the objective lens (PL APO 100×/1.40–0.7 oil, Leica Microsystems, Wetzlar, Germany). Two vortex phase plates (RPC Photonics, Rochester, NY, USA.) placed into the STED beams followed by a superachromatic quarterwave plate (600–2700 nm, B. Halle GmbH, Berlin, Germany) placed at the back of the objective lens afforded ring-shaped STED foci with a zero-intensity minimum in their center.

To ensure spatial overlap of the excitation and the STED foci, the diffraction patterns (‘point spread functions (PSFs)’) of the four beams were measured sequentially by recording scattered light from gold nanoparticles (80 nm) as they were scanned through the focal region. The alignment precision was on the order of 5 nm, i.e. below the resolution achievable with the setup.

Since all four laser beams originated from a single source, no pulse synchronization was necessary. Still, the simultaneous arrival of the excitation and the respective STED beam in the sample had to be adjusted by matching the optical path lengths for each pair of beams. On the contrary, the pairs of excitation and STED beams for the two color channels were time-shifted by about 40 ns using optical fibers of different lengths. This pulse-interleaved acquisition scheme enabled the (quasi-)simultaneous recording of both color channels: in addition to the spectral separation photons were assigned to a dye according to their arrival time at the detector. Due to the simultaneous recording of both color channels hardly any shift of the sample was possible during the recording time.

The fluorescence from the two fluorophores was separated from the laser beams with a custom made multiband dichroic mirror (Chroma Technology, Rockingham, VT, USA). It was subsequently split up with a second dichroic mirror (Z635RDC, Chroma Technology) according to the emission maxima of the different dyes, and was finally cleaned up with bandpass and longpass filters (M620/40, M670/40 nm and Z660LP, all from Chroma Technology). The fluorescence was then focused into separate multimode optical fibers (Ø = 62.5 µm, Thorlabs, Dachau, Germany) which served as confocal pinholes. The fibers were

#140586 - $15.00 USD Received 4 Jan 2011; accepted 18 Jan 2011; published 2 Feb 2011

attached to single-photon counting modules (SPC-AQRH-13-FC, Perkin Elmer, Salem, MA) which were connected to custom time gating electronics extracting the fluorescence signals following each of the excitation/STED pulse pairs. Optionally, for the acquisition of fluorescence lifetime data, the time trace of the fluorescent signals was measured by a time-correlated single-photon counting (TCSPC) module (SPC-730, Becker & Hickl GmbH, Berlin, Germany). Typically, images were acquired with pixel sizes of 20 nm × 20 nm and a pixel dwell-time of 1 ms. For the recording of lifetime STED images, the pixel dwell-time was increased to 3 ms to ensure a sufficient number of counted photons and thus appropriate statistics for lifetime analyses. In addition to the STED images, reference confocal images were recorded.

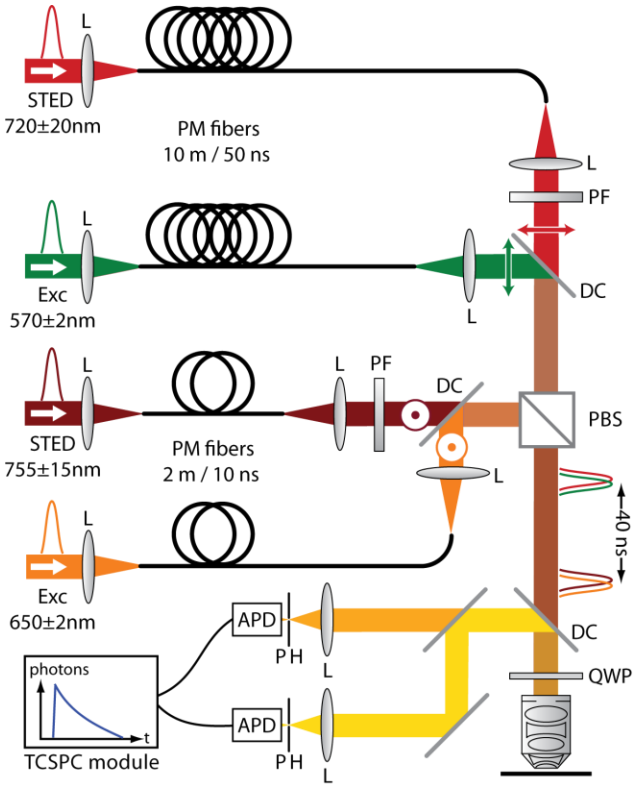

Fig. 1. Setup of the multi-lifetime/multi-color STED microscope.

2.2 Samples

Biological samples were mammalian PtK2 cells which were stained using an immunofluorescence protocol involving various primary antibodies (anti-alpha-tubulin rabbit IgG, anti-lamin A+C [131C3] mouse IgG and anti-clathrin goat IgG, Abcam plc, Cambridge, UK) and various labelled secondary antibodies (Jackson Immuno Research, West Grove, USA). The used dyes were ATTO 590 (donkey anti-goat), ATTO 647N (goat anti-rabbit) and KK 114 (sheep anti-mouse), respectively. Samples were fixated using methanol, as an embedding medium we used Mowiol with DABCO (1,4-diazabicyclo[2.2.2]octane) added as an antifading agent.

2.3 Channel separation by fluorescence lifetime

The lifetime of organic fluorophores is typically in the 2–5 ns range. When two dyes are selected from the upper and lower end of this range, respectively, the differences are usually sufficient to discriminate them by lifetime. A characteristic of STED microscopy is that the

#140586 - $15.00 USD Received 4 Jan 2011; accepted 18 Jan 2011; published 2 Feb 2011

initial part of the fluorescence decay is difficult to analyze as it is compromised by the action of the STED beam rendering the decay multiexponential. In other words, it contains contributions from fluorophores located further away from the doughnut zero, that have not been shut off by the (shorter action of the) STED beam. For this reason, this initial part does not contain information of the highest resolution [26]. After the STED beam has taken full action, the decay curve is largely given by the spontaneous fluorescence from the confined region around the center of the STED beam.

The model which we used to analyze the multiexponential fluorescence decay histogram is a generalization of the monoexponential model introduced in [27]:

$$g_j = N_g \left[\sum_{k=1}^{n} \left(A_k \frac{\mathrm{IRF}_j \otimes e^{jt/\tau_k} + c}{\sum_{l=1}^{N} \left(\mathrm{IRF}_l \otimes e^{lt/\tau_k} + c \right)} \right) + \left(1 - \sum_{k=1}^{n} A_k \right) \frac{b_j}{\sum_{l=1}^{N} b_l} \right]. \quad (1)$$

N is the number of histogram bins, n is the number of exponential decay components (one per dye was used), N_g is the total number of photons in the histogram, A_k is the amplitude of the k-th decay component, b_j is time-correlated background (e.g. Rayleigh or Raman scattering), c is constant background (e.g. detector dark counts), τ_k is the lifetime of the k-th dye, and t is the bin width. The model includes the convolution ($\otimes$) of the fluorescence decay with the instrument response function (IRF) which was measured by acquiring a TCSPC histogram from light scattered at gold nanoparticles. The time-correlated background b_j was taken from areas of the images where no fluorescent features were present. To fit the model function to the measured TCSPC histograms a custom routine was written in MATLAB (The Mathworks, Natick, MA, USA) which implements a maximum likelihood estimator (MLE) assuming Poissonian statistics [27]. The first two nanoseconds of the fluorescence decay were discarded and one exponential decay per dye was assumed. The lifetimes τ_k were determined from a fit once, and subsequently fixed by analyzing the image pixels. The per-pixel amplitudes A_k reflect the distribution of the two dyes. Since accurate analysis requires a certain signal level, a threshold was set, below which the analysis was not applied. Pixels with signal below the threshold were set to zero.

2.4 Spectral unmixing of STED images

The spectral separation of fluorescence from different dyes can be based on their emission and absorption spectra, or both. The first approach requires the fluorescence to be split with a dichroic beamsplitter in the detection path, to be properly filtered for each emission spectrum and to be detected with separate detection units. The image acquisition is not affected any further and, in particular, both color channels can be recorded simultaneously. This is not the case when the color separation is based on selective excitation where each dye is excited at a wavelength at which the other dye does not absorb. In this case, the individual color channels must be acquired sequentially.

However, the separation based on either of the two spectra alone is usually imperfect due to a more or less pronounced overlap between the absorption and fluorescence spectra of the dyes as a result of which fluorescence leaks into the respective cross channel. In STED microscopy, crosstalk may additionally arise due to the (weak) excitation of the dyes by the STED laser beams. The discrimination can be improved by combining selective excitation of the fluorophores together with a separation of their emission in which case the discrimination ratio is given by the product of the individual discrimination ratios. Then, only 2nd-order crosstalk remains (which arises when a dye A is excited and detected by the laser line and detection channel, respectively, that are assigned to a dye B). Appropriate data acquisition schemes can be realized by imaging the dye distributions one after another, each with the

#140586 - $15.00 USD Received 4 Jan 2011; accepted 18 Jan 2011; published 2 Feb 2011

appropriate pair of excitation light and spectral detection window in conjunction with intensity modulated excitation and lock-in detection [28,5]. Alternatively, one employs pulse-interleaved excitation and time-gated detection. Here we have chosen the latter approach.

Remaining crosstalk can be eliminated using linear unmixing which is well-established in widefield and confocal imaging; with slight modification, it also works for STED microscopy. When applying linear unmixing it is usually assumed that the signal in each pixel is a linear superposition of contributions from the different fluorophores [29]:

$$\mathbf{y} = \mathbf{E}\mathbf{x}. \tag{2}$$

Here, **x** and **y** are column vectors containing, for each pixel, the unknown fluorophore concentrations and the signals in the different detection channels, respectively. **E** is the sensitivity matrix whose elements ε_{ik} specify the relative sensitivity of detection channel *i* for dye *k* which can be determined from single-color reference measurements. The concentration values can be easily recovered by inverting the sensitivity matrix **E**.

The individual treatment of each pixel does not take into account that neighboring pixels are correlated, because the fluorophore distribution is convolved with the point-spread function (PSF). However, in conventional fluorescence imaging, the PSF is very similar for all color channels (except for its scaling with the wavelength) which permits the use of the single-pixel approximation.

In STED microscopy, the resolution is co-determined by the light-fluorophore interaction. As the cross sections for absorption and stimulated emission vary with wavelength, the effective PSF can be different for each combination of excitation and STED beams used. The image of a structure labeled with a particular fluorophore looks different in its dedicated detection channel as compared to its crosstalk found in the channel of a different fluorophore. In other words, channel unmixing also involves different spatial distributions, i.e. different point spread functions. Since it is not possible to use an individual pixel approximation, the formalism must be extended.

Let us assume a sample which contains structures labeled with *N* different fluorophores. For each fluorophore, a distinct combination of excitation and STED wavelengths as well as a dedicated detection channel is provided. Let $g_{kj}(\mathbf{r})$ denote the effective PSF applicable for fluorophore *k* subject to the illumination conditions *j*. The spatial distribution $x_k(\mathbf{r})$ of fluorophore *k* gives rise to a brightness distribution given by the convolution product $g_{kj}(\mathbf{r}) \otimes x_k(\mathbf{r})$. Then, the image $y_{ij}(\mathbf{r})$ observed in detection channel *i* is given by the weighted sum of contributions from all fluorophores $k = 1...N$:

$$y_{ij}(\mathbf{r}) = \sum_{k=1}^{N} \varepsilon_{ik} \left[g_{kj}(\mathbf{r}) \otimes x_k(\mathbf{r}) \right] \tag{3a}$$

or, in matrix notation:

$$\mathbf{Y}(\mathbf{r}) = \mathbf{E}\mathbf{X}(\mathbf{r}). \tag{3b}$$

Here, the element ε_{ik} of the matrix **E** contains the sensitivity of detection channel *i* for dye *k*. Equation (3)b) has the same form as Eq. (2), except for the vectors **x** and **y** which have been replaced by the matrices $\mathbf{X}(\mathbf{r}) = \mathbf{g}(\mathbf{r}) \otimes \mathbf{x}(\mathbf{r})$ and $\mathbf{Y}(\mathbf{r})$. Therefore, in order to invert Eq. (3)b) and to retrieve the single channel images $\mathbf{X}(\mathbf{r})$, the full matrix $\mathbf{Y}(\mathbf{r})$ must be recorded, including the cross channels $y_{ij}(\mathbf{r})$ (i ≠ j). Then,

$$\mathbf{X}(\mathbf{r}) = \mathbf{E}^{-1}\mathbf{Y}(\mathbf{r}) \tag{4}$$

is easily calculated.

#140586 - $15.00 USD Received 4 Jan 2011; accepted 18 Jan 2011; published 2 Feb 2011

We decided to implement a pulse-interleaved illumination scheme with the two pairs of excitation/STED pulses shifted in time by 40 ns, each of which marking the beginning of a time window. By applying a synchronized electronic time gating, the detector signals were acquired separately for each time window, thus yielding (for each detection channel) a recording for each combination of excitation and STED lasers, i.e. the elements of the matrix $\mathbf{Y}(\mathbf{r})$ in Eq. (4). The pulse-interleaved scheme allowed us to record both channels (quasi) simultaneously, i.e. with no time delay in between the color channels. As a result, any drift between the color channels is excluded.

In order to perform the linear unmixing the sensitivity coefficients ε_{ik} had to be determined for the combination of dyes and optical filters used in our implementation. To this end, monolabeled samples were used, featuring microtubules stained either just with ATTO 590 or with KK 114. The fractions of the fluorescence signals detected in the cross channels were found to be 0.12 and 0.26, respectively. Therefore,

$$\mathbf{E} = \begin{pmatrix} 1 & 0.12 \\ 0.26 & 1 \end{pmatrix}, \ \mathbf{E}^{-1} = \begin{pmatrix} 1.03 & -0.124 \\ -0.268 & 1.03 \end{pmatrix} \tag{5}$$

In the discussion of crosstalk analysis one must further consider that, as a matter of principle, TCSPC electronics can only detect a single photon per synchronization pulse. Therefore, when a photon is detected in the first 40 ns time window, a second photon cannot be sensed in the following window. The signals in the two gating windows are therefore correlated to some extent. In principle, this limitation can be overcome by feeding a synchronization pulse to the TCSPC card for each time window. However, due to the dead time of 180 ns of the TCSPC card, a photon in the second time window still remains undetected if another one had been detected in the first. To remove all constraints, four independent TCSPC units would be needed. Finally, the dead time of the APDs (~30 ns) is below the width of the gating windows; hence, it does not affect the counting in the second window. Since a quadruple TCSPC unit was not available for our experiments, we ensured having photon count rates much below the counting limit of the module.

3. Results & discussion

3.1 Two-channel STED imaging: fluorescence lifetime separation

As a proof of principle, we first applied our lifetime separation algorithm to single-color labeled samples, namely tubulin immunolabeled with ATTO 647N and KK 114, respectively (Fig. 2A). By analyzing the data of the monolabeled samples the fluorescence lifetimes were determined as (1.8 ± 0.6) ns for ATTO 647N and (3.1 ± 0.5) ns for KK 114; the degree of labeling (DoL), i.e. the number of fluorophore molecules per secondary antibody was 4 and 2, respectively.

Because we noted significant changes in the fluorescence lifetimes of KK 114 and ATTO 647N, depending on the secondary antibody the dyes was attached to, we also checked the fluorescence lifetime when the labeled secondary antibodies were attached to primary antibodies targeted to different cellular structures in the cell (tubulin, vimentin, clathrin, lamin, the Golgi apparatus, endosomes and lysosomes). We found that, throughout these targets, the fluorescence lifetime remained constant to within 0.2 ns, which is on the same order as the statistical spread of lifetimes found in a single staining.

#140586 - $15.00 USD Received 4 Jan 2011; accepted 18 Jan 2011; published 2 Feb 2011

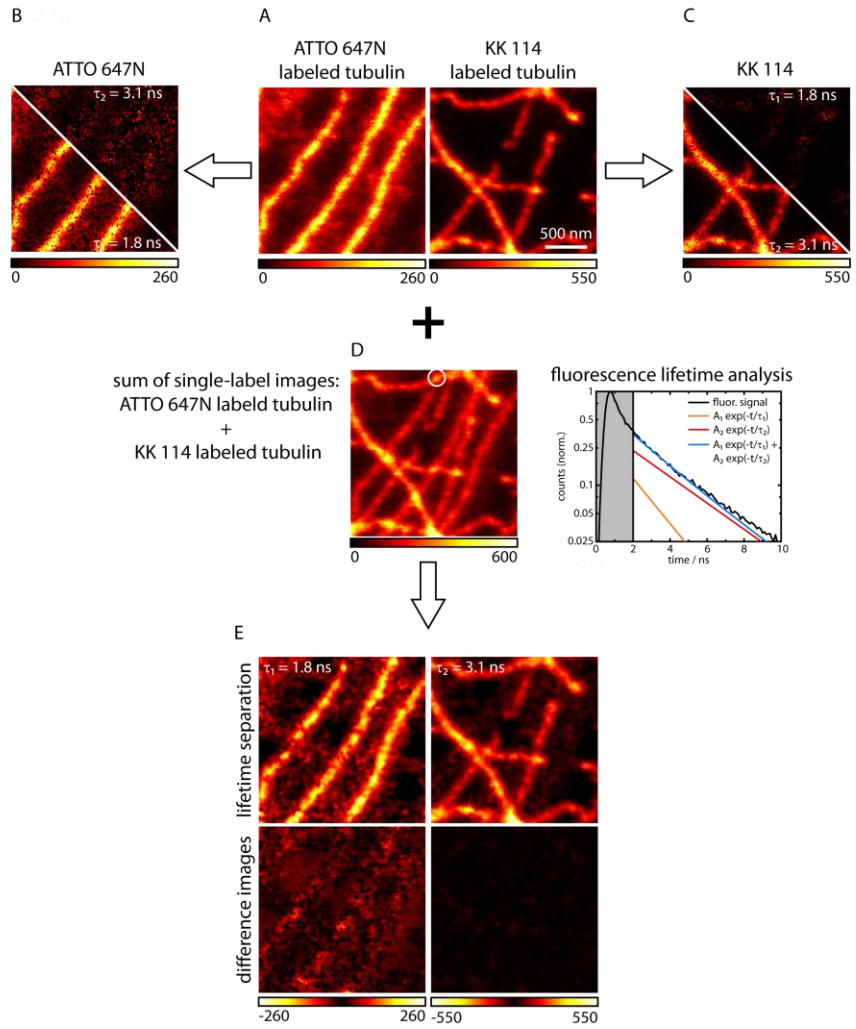

Fig. 2. Fluorescence separation by lifetime analysis. Images of tubulin labeled with ATTO 647N (left) or KK 114 (right) were recorded by TCPSC (A). A per-pixel monoexponential fit of the lifetime histogram reproduces the original images with residuals < 10% (B, C). Even after adding the photocounts of the original recordings (D) the two channels can be recovered by fitting a biexponential function to the lifetime histograms: (E) shows the amplitude images (top) of the two lifetime components along with the corresponding difference to the initial data (bottom).

In order to verify the suitability of this dye combination for multi-lifetime imaging we fitted the lifetime data with a biexponential decay with fixed decay times of 1.8 ns and 3.1 ns, respectively. The resulting amplitude images are shown in Fig. 2B and C. As the images demonstrate, the bulk of the signal is assigned to the correct dyes, and only a fraction < 10% is found in the cross channels. Also, to emulate a dual-color-labeled sample, we added the lifetime histograms of both (separately recorded) images of the single-color labeled samples (Fig. 2D) and then applied the lifetime-based image decomposition. As shown in Fig. 2E, the algorithm is able to separate the lifetimes well (upper panel) which is corroborated by negligible residuals (lower panel).

Finally, the analysis was applied to a double-labeled sample in which lamin and tubulin were labeled with KK 114 and ATTO 647N, respectively. Figure 3A shows the raw intensity image in which the structures are overlapping in space. After fitting the lifetime histogram for

#140586 - $15.00 USD Received 4 Jan 2011; accepted 18 Jan 2011; published 2 Feb 2011

each pixel with a biexponential decay of fixed lifetimes of 1.8 ns and 3.1 ns, the two structures are well separated in the resulting amplitude images (Fig. 3B).

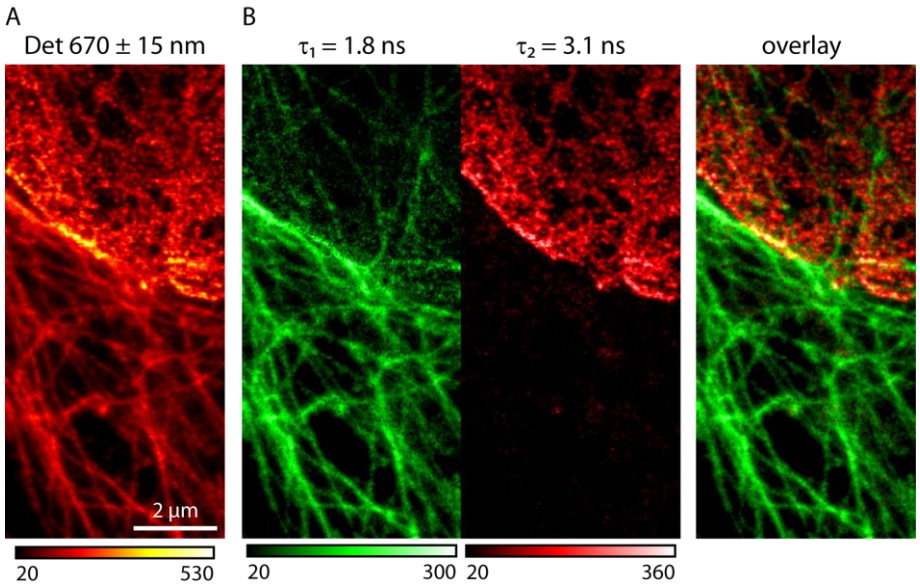

Fig. 3. Two-channel STED imaging by fluorescence lifetime separation. Tubulin and lamin were immunostained with ATTO 647N and KK 114, respectively. (A) Raw intensity STED data and (B) channels decomposed by lifetime separation (green: tubulin, red: lamin).

3.2 Extension to three-channel STED imaging

Dual-color STED imaging with spectral discrimination has been shown earlier [30]. Since, from those experiments, our STED microscope was pre-equipped for two-color operation we were able to combine lifetime and spectral separation to perform three-channel STED imaging with resolution not fundamentally limited by diffraction. To this end, we used two dyes with similar spectral properties but different lifetimes (KK 114, ATTO 647N) and a third dye with a different absorption and fluorescence spectrum (ATTO 590) to label the proteins lamin, tubulin, and clathrin in the same sample of human glioblastoma cells, respectively. Figure 4 shows an example of triple-color STED imaging along with the corresponding confocal image. While the structure of clathrin was separated from the other ones utilizing the different spectral properties of ATTO 590, the structures of lamin and tubulin were separated by lifetime analysis.

The simultaneous recording of all channels ensures that neighboring structures are imaged within a short time period rather than on a frame-by-frame basis. This minimizes drift and/or motion artifacts which may impair the colocalization accuracy especially in live cell imaging.

#140586 - $15.00 USD Received 4 Jan 2011; accepted 18 Jan 2011; published 2 Feb 2011

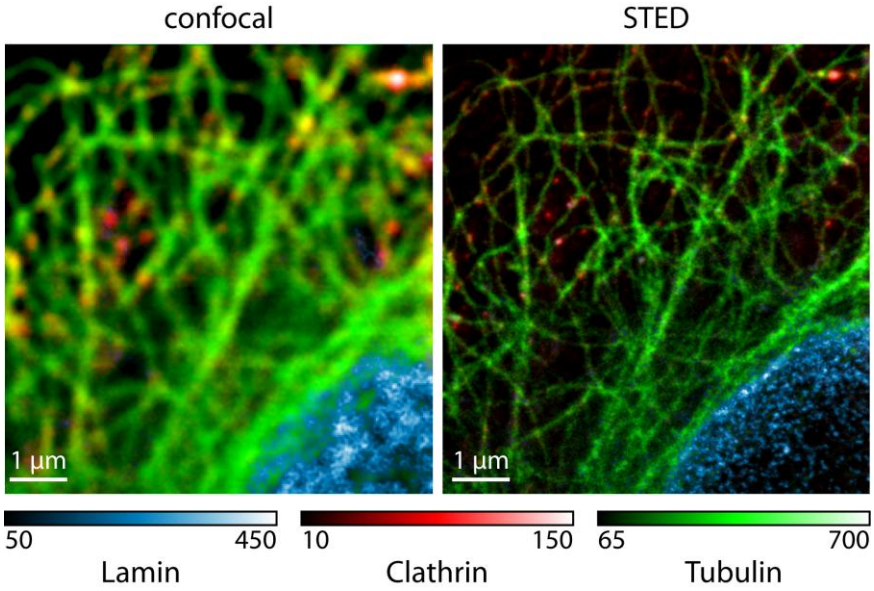

Fig. 4. Combined spectral and lifetime separation. Lamin and tubulin were stained with KK 114 and ATTO 647N, respectively, which were segregated by lifetime analysis. The ATTO 590 fluorescence (clathrin) was spectrally separated from those of the other dyes.

3.3 Improvement of the colocalization accuracy

Unlike the lifetime based image separation the discrimination by wavelength relies on the use of two pairs of excitation/STED beams and on two separate detection paths. Therefore, the colocalization accuracy critically depends on the precision with which the beams are superimposed and on potential drifts. By imaging dual-color fluorescent beads (FluoSpheres® amine-modified microspheres, 200 nm, red fluorescent, Invitrogen GmbH; additionally labeled with ATTO 647N) we estimated the drift between the images which finally limits the localization analyses. With our experimental configuration we observed a drift of ~0.01 nm/min and a maximum of 10 nm over 12 h which sets a limit for colocalization measurements.

During the course of the experiments, a new prototype laser source became available which allowed us to set up another STED microscope. The laser source (by Fianium Ltd., Southampton, UK) provides a supercontinuum output and two additional high-power outputs at fixed wavelengths of 711±2 nm and 742±2 nm (pulse length of ~100 ps, pulse repetition rate of 20 MHz, pulse energy of 30–40 nJ). The new setup prompted us to review the previous design, resulting in a slightly changed beam path with improved colocalization performance (Fig. 5). Rather than combining the excitation/STED pairs after the fiber outputs both STED beams are combined first and coupled to a common optical fiber. In doing so, the STED beams are intrinsically locked together along their way through the microscope and are immune to drift with respect to each other. In the same way, the excitation beams were coupled to a common optical fiber. Finally, the detection unit was modified by introducing a single pinhole for both fluorescence channels and by splitting up the fluorescence after this common pinhole. This configuration ensures that the two detection PSFs are locked in space. Finally a commercial beam scanning unit (Yanus IV Digital Scan Head, TILL Photonics GmbH, Munich, Germany) was introduced into the setup to enable faster scanning. As before, the excitation/STED pulse pairs were temporally separated but, due to the higher repetition rate (20 MHz, corresponding to a pulse-to-pulse interval of 50 ns) a delay of only ~25 nm was used.

#140586 - $15.00 USD Received 4 Jan 2011; accepted 18 Jan 2011; published 2 Feb 2011

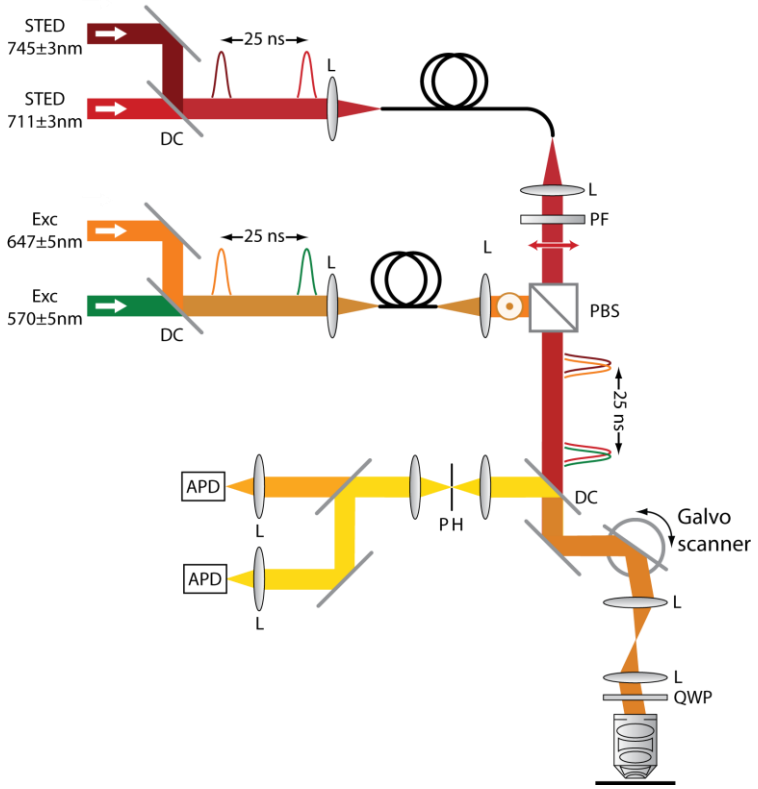

Fig. 5. Improved beam path configuration for dual-wavelength STED imaging. Contrary to the previous design the STED beams are jointly coupled to a single mode optical fiber and are guided to the same phase plate.

In a strict sense, the coupled STED beams require a special achromatic phase plate, having nearly equal performance at 711 nm and 742 nm. However, simulation shows that the effect of the vortex phase plate is very robust with respect to minor changes in wavelength. For the design wavelength (688.9 nm) of the phase plate in use, we calculated that the minima of the focal doughnuts should experience a shift by ~10 nm, while the depth of the minima remains almost unchanged. We confirmed the calculation by scanning the focal doughnuts with gold nanoparticles and found that the doughnut minima were negligible, i.e. zero within experimental accuracy. We also found a slight offset of ~27 nm between the zero intensity points which, however, was not exclusively caused by the phase plate, because an offset of 14 nm was observed even between the regularly focused spots (when the phase plate was removed). Since such an offset is not expected for beams propagating on the optical axis, we tried out different lenses of the same type. We found that the offsets strongly depended on the individual lens used. We therefore conclude that lateral chromatic aberrations are innate to the objective lens, originating from alignment imperfections introduced during lens assembly. However, since for a rigidly mounted lens the offset is constant, the images in the two color channels can be shifted accordingly.

To validate the alignment and drift insensitivity of the setup we further recorded dual-color labeled fluorescent beads (FluoSpheres®: carboxylate-modified microspheres, 40 nm, red and dark red fluorescent, Invitrogen GmbH) over a period of several hours. In each of the spectrally separated images 50-100 beads were independently localized by calculating the centroid of their fluorescence image. From the positions, the offset of each bead in the two images was determined (Fig. 6). By averaging over the bead positions, the mean shift between the images was obtained. The results show an offset of 24 nm between the images which, however, remains <10 nm over a period >24 hours.

#140586 - $15.00 USD Received 4 Jan 2011; accepted 18 Jan 2011; published 2 Feb 2011

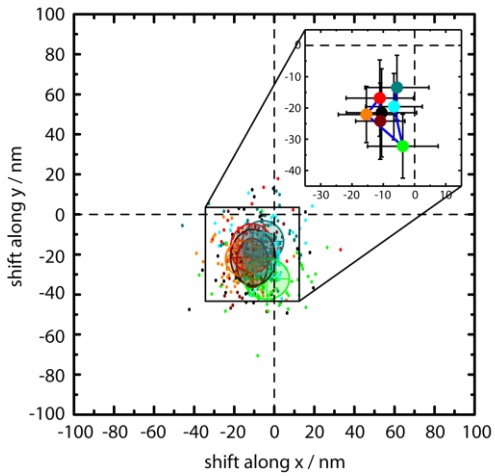

t	x / nm	y / nm
0 h	-11 ± 11 nm	-22 ± 14 nm
1 h	-11 ± 7 nm	-24 ± 12 nm
2 h	-11 ± 11 nm	-17 ± 12 nm
19 h	-15 ± 9 nm	-22 ± 9 nm
20 h	- 4 ± 11 nm	-32 ± 10 nm
22 h	- 7 ± 9 nm	-22 ± 14 nm
27 h	- 6 ± 10 nm	-13 ± 10 nm

Fig. 6. . Stability of the dual-wavelength colocalization measurements. The main scatter plot shows the offset of individual beads between the two color channels at various times. The inset shows the image offset as obtained by averaging over the individual offsets. Over the whole measurement period the offset remains constant to within the statistical error of the experiment.

4. Conclusion and outlook

We introduced a combined multi-lifetime/multi-color STED microscope optimized for colocalization experiments with up to three colors. Using two far-red dyes (ATTO 647N, KK 114) we were able to separate their emission based on a difference of their fluorescence lifetime of ~1.3 ns (when bound to a secondary antibody). The separation by lifetime requires only a single STED beam and is therefore not subject to thermal drift between beams. Furthermore, the localization accuracy is not compromised by dipole orientation artifacts as are single-molecule localization techniques. The single-beam STED approach conceptually provides the best colocalization accuracy. The organic dyes in our experiment allowed us to perform the lifetime separation with < 10% crosstalk.

Three-channel operation was accomplished by adding a second pair of excitation/STED beams tailored to a third dye (ATTO 590). By coupling the STED beams into a common optical fiber we excluded any drift between the STED beams which is otherwise the main source of colocalization error. While a constant offset between the STED focal doughnuts was observed due to lateral chromatic aberrations in the objective lens, this shift proved to be remarkably constant over time thus allowing reliable colocalization measurements even for long measurements. In the future it will be rewarding to identify or develop further dyes that can be matched for three, four, or more channel recordings. We also note that with appropriate modifications, the approach discussed herein can also be extended to STED-related far-field optical nanoscopy concepts, such as ground state depletion and the generalized RESOLFT concept utilizing photoswitchable fluorescent proteins.

It is also important to realize that multichannel separation by color or lifetime fundamentally benefits from any increase in spatial resolution: the higher the spatial resolution, the more relevant the discrete nature of the sample becomes, causing fewer emitters to overlap randomly in signal. It should also be kept in mind that the turning off of adjacent fluorophores by STED increases the molecular specificity of the signal thus facilitating separation. Providing signal just from a narrow coordinate in space, an ideal ultrahigh resolution STED or RESOLFT type of microscope relays the fluorescence either from a single spatially isolated or from two or three colocalizing fluorophores that are occupying the same tiny coordinate range targeted by the (doughnut) beam featuring the intensity zero. In this ultimate case, separation is possible with a minimum number of photons and the images instantly provide the ultimate colocalization information.

#140586 - $15.00 USD Received 4 Jan 2011; accepted 18 Jan 2011; published 2 Feb 2011

Finally, we note that, alternatively, one can also use the application of multiple labels as a means to increase the imaging speed in subdiffraction resolution imaging by the same factor. Altogether, our study shows that improving subdiffraction resolution and developing multichannel recording is a highly synergistic development holding great potential in the near future.

Acknowledgments

We thank Dr. E. Rothermel for assistance with the sample preparation and immunolabeling, Dr. K. Kolmakov and Dr. V. Belov for providing the dye KK 114 and J. Jethwa for proofreading of the manuscript. The research leading to these results has received funding from the European Community's Seventh Framework Programme FP7/2007-2011 under grant agreement no. 201837.

#140586 - $15.00 USD Received 4 Jan 2011; accepted 18 Jan 2011; published 2 Feb 2011